

AIAA 04–22666

**Modelling the Ballistic Missile
Problem**

**with the State Transition Matrix:
A Comparative Analysis**

Justin S. McFarland

Virginia Tech, Blacksburg, VA 24061

**AIAA Region I-MA Student Conference
April 16–18, 2004/Blacksburg, VA**

Modelling the Ballistic Missile Problem with the State Transition Matrix: A Comparative Analysis

Justin S. McFarland*
Virginia Tech, Blacksburg, VA 24061

The ballistic missile problem is a typical topic of discussion in introductory astromechanics courses when discussing Keplerian motion. This study revisits the introductory ballistic missile problem by including the spherical Earth, rotation, and addition of atmospheric drag. The scope of this exercise comprises launching from an initial set of coordinates in the form of latitude and longitude in Earth frame to a desired target set of coordinates. As intuition suggests, resolving the target location increases in difficulty as the model complexity increases. Further, when a significant atmosphere is introduced, analytic solutions are no longer possible using traditional methods. Modern techniques are then explored using the state transition matrix, a sensitivity based tool, to correct the initial velocity guess in order to converge upon the desired target within a specified accuracy. An analytical solution of the two-body problem and a numerical approach are used to compute the state transition matrix. A comparison is made to determine the regions of convergence available to each of these techniques, in order to determine their usefulness in the form of number of iterations required to converge, trends if the solutions did not converge, and computational speed.

Nomenclature

a	Semimajor axis, km
f	True anomaly angle, rad
h	Altitude above surface, km
p	Semilatus rectum, km
r	Trajectory radius, km
V	Trajectory velocity, km/s
Δt	Time of flight, s
ΔV	Change in velocity, km/s
Φ	State transition matrix
β	Modified ballistic coefficient, kg/km ²
δr_f	Range error, km
δv	Velocity correction, km/s
λ	Atmosphere scale height, km
μ	Gravitational parameter, km ³ /kg ²
ρ	Density, kg/km ³

Subscripts

x, y, z	Cartesian body axes, km
f	Final state
ref	Reference state
0	Initial state on surface

Superscripts

t	target
-----	--------

Introduction

THE ballistic missile problem is typically represented in introductory astromechanics texts as

*Student Member

Copyright © 2004 by Justin S. McFarland. Published by the American Institute of Aeronautics and Astronautics, Inc. with permission.

a simplified planar two-body problem with a non-rotating Earth. From this information we can usually determine the range of a projectile, the initial flight path angle, the orbit eccentricity and semi-major axis, and its true anomaly angles at launch and impact. It is of interest to expand upon this basic model in order to add realism to the problem.

Applications desiring increased complexity include determining the initial launch vector direction and velocity requirements for a vehicle, simulation of the ground track of a hypersonic vehicle, orbit plane determination, analysis of energy required at various launch sites to reach different targets, and means to determine potential load factors, deceleration, and temperature gains of a body as it travels through the atmosphere. Additionally, interplanetary missions such as those to Mars and Venus may require high degree of landing accuracy when entering their respective atmospheres. Thus hyperbolic trajectories can also be utilized in order to resolve an appropriate, necessary velocity at a fixed point in space. This provides the ballistic unpowered free-flying point mass trajectory¹ to arrive in the locale of the target and then use a guidance system to make fine adjustments. In order to make the necessary adjustments to the increased realism, the complexity of our system must be increased in order to account for motion in a inertial, cartesian coordinate frame.

To meet the need of this complexity, it is of further interest to utilize the power of modern computers in order to rapidly account for perturbations such as J_2 and atmospheric drag and the effects due to the rotation of the primary body. Numerical integration

techniques can be employed to account for effects such as those of a thrusting projectile through an atmosphere, the drag and lift on this body, and relevant effects of J_2 and other perturbations² of these problems. However, when perturbation methods are taken in to account, resolving the trajectory of the vehicle to arrive at a specified target is no longer a function of Keplerian motion. Modern techniques must be invoked in order to resolve the more complex dynamics of these systems. One such technique is the use of the state transition matrix (STM).

The state transition matrix is a powerful sensitivity based tool that can be used to assist in the correction of an initial guess of velocity.² The STM can be used to formulate the necessary launch criteria for a ballistic missile in order to make the necessary corrections to hit a target when adjusting to a variety of perturbation methods. The STM can be formulated either through the analytic solutions of motion or accounted for directly by using a numeric sensitivity technique.

This document will show the correlation between the analytical solution and a numerical solution in computing the STM for the advanced ballistic missile problem. A comparison will also be made in the computational effort and trends of convergence or divergence between the two methods for a series of launch points to a fixed array of globally dispersed targets.

Methods within the STM

The state transition matrix provides a method for mapping the initial state vector of a system to a final state vector at any particular time. Corrections for perturbations such as J_2 , J_4 , and drag must be made in order to minimize error on trajectories.

There are two primary methods for computing such corrections: the analytic solutions for determining where a body will be given an initial guess as well as the final portion of the initial guess; and the numerical solution where by a sensitivity of the trajectory to small velocity changes from the initial guess are computed.

Analytic Method

The analytic method³ employs the special case compilation of terms from the F and G method of propagating a 2-body problem, or Keplerian motion, found in Equation 1.

$$[\Phi] = \frac{r_0}{\mu} \cdot (1 - F) \left(\begin{bmatrix} \Delta r_x \\ \Delta r_y \\ \Delta r_z \end{bmatrix} \begin{bmatrix} V_{0x} & V_{0y} & V_{0z} \end{bmatrix} - \begin{bmatrix} \Delta V_x \\ \Delta V_y \\ \Delta V_z \end{bmatrix} \begin{bmatrix} r_{0x} & r_{0y} & r_{0z} \end{bmatrix} \right) + \frac{C}{\mu} \left(\begin{bmatrix} V_x \\ V_y \\ V_z \end{bmatrix} \begin{bmatrix} V_{0x} & V_{0y} & V_{0z} \end{bmatrix} \right) + G \begin{bmatrix} 1 & 0 & 0 \\ 0 & 1 & 0 \\ 0 & 0 & 1 \end{bmatrix} \quad (1)$$

Where F and G are the terms from the F and G solution represented in 2, 4, and 3; and C is represented in Equation 5.

$$F = 1 - \frac{r}{p}(1 - \cos(\Delta f)) \quad (2)$$

$$\dot{F} = \sqrt{\mu p} \tan\left(\frac{\Delta f}{2}\right) \left(\frac{1 - \cos(\Delta f)}{p} - \frac{1}{r_0} - \frac{1}{r} \right) \quad (3)$$

$$G = \frac{r_0 r \dot{F}}{\sqrt{\mu a}} \quad (4)$$

$$C = a \sqrt{\frac{a^3}{\mu}} (3 \sin(\hat{E}) - (2 + \cos(\hat{E}))\hat{E}) - \Delta t a (1 - \cos(\hat{E})) \quad (5)$$

$$\hat{E} = \arctan\left(\frac{\frac{-r_0 r \dot{F}}{\sqrt{\mu a}}}{1 - \frac{(1-F)r_0}{a}}\right) \quad (6)$$

Where \hat{E} is the modified eccentric anomaly in Equation 6, a is the semimajor axis, p is the semilatus rectum, f is the true anomaly angle, and Δt is the flight time of the projectile.

Now that we have the state transition matrix $[\Phi]$, we can now determine our range error $\delta \mathbf{r}_f$ of final position vector from where we end up, \mathbf{r}_f from where we should be, \mathbf{r}_f^t , in Equation 7.

$$\delta \mathbf{r}_f = \mathbf{r}_f - \mathbf{r}_f^t \quad (7)$$

With $[\Phi]$ and $\delta \mathbf{r}_f$ we can backsolve to find the necessary velocity correction vector, $\delta \mathbf{v}$ as shown in Equation 8.

$$\delta \mathbf{v} = [\Phi]^{-1} [-\delta \mathbf{r}_f] \quad (8)$$

The velocity corrected vector $\delta \mathbf{v}$ is then added to the initial cartesian velocity vector set to correct for the effects of the perturbation. After successive iterations of recomputing the final location of the trajectory after

applying the correction, the error vector $\delta \mathbf{r}_f$ is driven to zero when the solution converges; else it diverges. It is observed that for successive increases in error, the solution will diverge and the case cannot be resolved just by using this method. For cases where the solution diverges or converges slowly the numerical STM can be employed.

Numerical STM

The numerical STM is determined by adding small changes in velocity to the initial cartesian parameter set.² These changes are represented as vector quantities. For instance 9 demonstrates a small change, v_ϵ in velocity in the cartesian x direction where v_ϵ is 0.001 km/s.

$$\delta \mathbf{v}_1 = [v_\epsilon \ 0 \ 0] \quad (9)$$

A change in each of the cartesian directions is added to the input cartesian set. Each is then propagated for a predetermined flight time whereby a final location is resolved for the three perturbed cases. These final locations are then compared to the unperturbed velocity cartesian parameter set location as depicted in Figure 1.

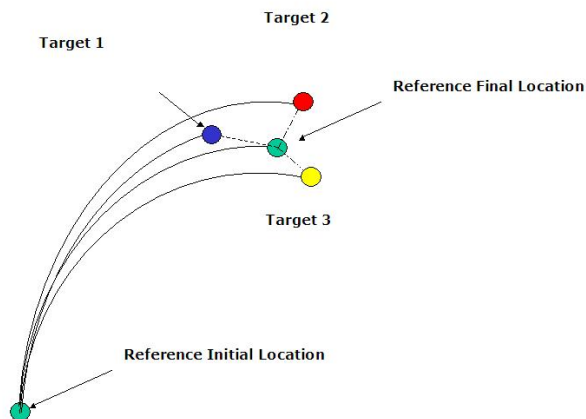


Fig. 1 Numerical STM compares a reference trajectory final location to 3 perturbed trajectories.

Sensitivities are then derived by dividing the change in range over the magnitude of perturbed velocity change. Equation 10 indicates the calculation for the first column of the STM. Here, Target i , for $i = 1, 2, 3$, from Figure 1 is indicated as \mathbf{r}_f^i and the reference final location is \mathbf{r}_{ref} .

$$\begin{pmatrix} \frac{\delta r_x}{\delta v_1} \\ \frac{\delta r_y}{\delta v_1} \\ \frac{\delta r_z}{\delta v_1} \end{pmatrix} = \frac{\mathbf{r}_f^i - \mathbf{r}_{\text{ref}}}{v_\epsilon}. \quad (10)$$

The numerical sensitivity matrix is then formed as shown in Equation 11 by utilizing the three target locations formed by propagating the perturbed initial conditions along the flight time.

$$[\Phi] = \begin{bmatrix} \frac{\delta r_x}{\delta v_1} & \frac{\delta r_x}{\delta v_2} & \frac{\delta r_x}{\delta v_3} \\ \frac{\delta r_y}{\delta v_1} & \frac{\delta r_y}{\delta v_2} & \frac{\delta r_y}{\delta v_3} \\ \frac{\delta r_z}{\delta v_1} & \frac{\delta r_z}{\delta v_2} & \frac{\delta r_z}{\delta v_3} \end{bmatrix} \quad (11)$$

Problems using the numerical STM involve the creation of a singular matrix. These singularities are introduced when the sensitivity in range is computationally negligible with respect to the small change in velocity. These instances can occur when the projectile is sent on a hyperbolic trajectory. Further, we must use constant flight time when using the numerical STM. Propagators can be set up in order to utilize the constraint of the surface in order to determine a time of impact. With perturbations in velocity, the flight time for each case will differ. This would imply that the STM is also a function of time, which it is not. Instead, a constant flight time propagation technique must be invoked regardless of whether the projectile's final perturbed position is above or below the surface. However, to determine the reference position of the projectile, \mathbf{r}_{ref} , the trajectory is propagated until a surface hit is observed. This assures that the projectile will hit the surface if not on an escape trajectory and thus all solutions are found in a ring on the surface and not just within a sphere.

Problem Definition

It is desired to formulate the necessary initial conditions of velocity for a given initial surface location and a desired final target location in the Earth fixed frame of reference. The initial position and velocity vectors are then propagated throughout the flight time of a simulated point-mass projectile until impact. An initial guess is computed using the Keplerian two-body solution for flight time and initial velocity. This guess is then subjected to the state transition matrix technique and velocity corrections are applied. In order to determine a measure of effectiveness for each type of state transition matrix a host of targets dispersed globally is composed and convergence criteria such as number of iterations to converge (if at all) and computational time is compared for a variety of launch locations.

Non-Keplerian Effects

Numerous non-Keplerian motion effects can be added to increase the fidelity of the ballistic missile problem model. Some of the major effects due to the environment will be resolved in this study including planetary rotation and the atmosphere on a simple projectile with a defined ballistic coefficient. This projectile will not have a defined an inertia tensor nor will lift be modelled.

Rotation

Planetary rotation is a significant source of error for projectiles with long flight times. As the body ro-

tates, the target itself will move. For minimum energy 2-body trajectories, the flight time can remain constant, and a new trajectory computed to essentially lead the target.⁴ However, since the purpose of these simulations is to build tools capable of resolving higher fidelity solutions, the minimum energy transfer time is not used to form solutions; it is used as an initial guess only.

Atmosphere

A piece-wise exponential model was selected from previous work,⁵ to represent the atmosphere. It is assumed that an exponential density model can accurately represent the atmosphere.^{1,6,7} The nature of exponential atmosphere density model provides the ability to estimate the density at altitude and obtain closed-form solutions while maintaining reasonable accuracy. For sea-level conditions we assume a initial density, ρ_0 of $1.225 \times 10^9 \text{ km}^3$.

For this exponential model the term Γ will be used to represent the density ratio at altitude as shown in 12.

$$\Gamma = \frac{\rho}{\rho_0} = e^{-\frac{h}{\lambda}} \quad (12)$$

The piecewise function changes properties at 152 km altitude (500,000 ft.) For the upper segment of the piecewise function, the reference density ratio at $1.524 \times 10^2 \text{ km}$ is 1.4848 kg/km^3 . A scale height, λ for elevations from 0 to 152 km is 6.882 km. For 152 km and above, 83.887 km is used.

This study invokes the atmosphere at 122 km (400,000 ft.) on the rising portion of the trajectory through the descent phase to the surface. It is assumed the the trajectory on the ascending portion to this location follows a Keplerian trajectory using thrust to match the necessary conditions when drag begins to be modelled.

Projectile Definition

The next task is to model a vehicle. This vehicle has three key parameters that we must know in order to determine the influence of drag acceleration. They are mass, representative area, and drag coefficient. In many cases all three of these parameters are not constant. A vehicle with an ablative heat shield will lose mass; a vehicle could deploy speed brakes or a parachute to increase area; drag coefficient is generally a function of lift coefficient. For our discussion, we model a ballistic missile, thus we neglect lift terms and consider drag to be much greater than lift.

When mass: m , area: S , and drag coefficient: C_D are combined they represent a term called the ballistic coefficient,⁸ β . This is represented as $\frac{m}{C_D \cdot S}$, and is traditionally in units of kg/m^2 .

To maintain unit consistency throughout the simulation, we will redefine the units as kg/km^2 . The ballistic parameter, β for satellites is considered low⁸

at values of $20 \times 10^6 \text{ kg/km}^2$ and high for $200 \times 10^6 \text{ kg/km}^2$. Feathers for instance have a very low ballistic parameter, while a battleship projectiles and ballistic missiles have a large values. This is the parameter that defines how well a projectile can penetrate the atmosphere.⁹ For the purposes of this study, four values of β are chosen in $\frac{\text{kg}}{\text{km}^2}$: ∞ , to indicate that the projectile is unaffected by the atmosphere; 2×10^{12} ; 2×10^9 , and 200×10^6 . Realizing that these values are not wholly representative of probable objects, but fundamental to the examination of the introduction of the effects of drag to the problem. Next we determine the method in which we model drag.

Modeling Drag

The drag force is generally defined¹ as in Equation 13.

$$D = \frac{1}{2} \rho v^2 C_D S \quad (13)$$

Where D is drag force and v is velocity magnitude. To incorporate the more advanced vector form of acceleration, we divide by mass and multiply by the negative velocity direction unit vector as shown in Equation 14.

$$\mathbf{a}_{\text{Drag}} = \frac{1}{2} \rho (\mathbf{v} \cdot \mathbf{v}) \frac{C_D S}{m} \frac{(-\mathbf{v})}{\|\mathbf{v}\|} \quad (14)$$

Next we simplify the equation and incorporate β in 15.

$$\mathbf{a}_{\text{Drag}} = \frac{\rho}{2\beta} (\mathbf{v} \cdot \mathbf{v}) \frac{(-\mathbf{v})}{\|\mathbf{v}\|} \quad (15)$$

Now that drag and the projectile are defined, the target array is defined.

Array of Targets

An array of targets was formulated using a grid work of points in latitude and longitude. Initial studies including rotation utilize a 703 point array ranging from 90° N latitude to 90° S latitude in increments of 10° . A longitudinal grid from -180° to 180° E is formulated also using increments of 10° . For cases employing drag, a much smaller grid size of 49 points is used due to the much heavier computational requirements. This grid is defined from 90° N to 90° S in increments of 30° with longitude from 90° W to 90° E by increments of 30° . The grid size reduced in longitudinal span to eliminate the large errors associated with the two-body solution initial guess.

Array of Launch Locations

Launch locations were chosen with strict regard to the assumption of symmetry across the equator. The initial locations of the representative launch locations are chosen to be 0° N by 0° E , 45° N by 0° E , and 90° N by 0° E .

Comparison of STMs

The primary means of comparing the numerical and analytical STM effectiveness is chosen to be the number of iterations required to correct the velocity. The number of iterations results in the indirect comparison of the computational power required in order to resolve a solution. An outline of the program created to solve the problem is shown in Figure 2.

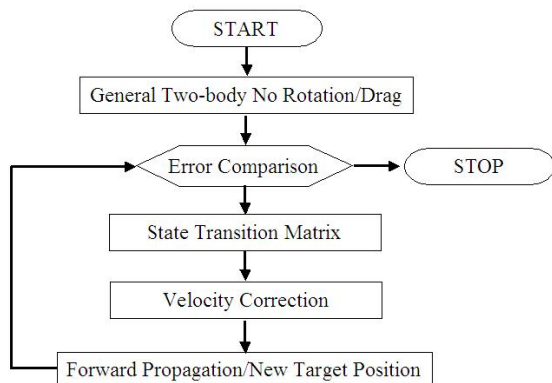


Fig. 2 Iterative approach used to resolve solution.

The program receives inputs of launch site and target site initial conditions. The two-body no-rotation solution is then processed. A flight time and initial cartesian coordinate set are outputted to a propagator to create the full trajectory profile. This is then outputted to the STM of choice. The error of the rotated target to the final projectile's location after the time of flight is compared in the while loop. If the error is not within an acceptable tolerance, the velocity is corrected. The number of iterations represents the number of times correcting the velocity of the cartesian coordinate set.

It was chosen that 10 iterations would be allowed for velocity corrections to resolve the target solution within an accuracy of 1.6 km (recall this error is a linear error that is the direct subtraction of vectors from the target location to the final location of the projectile). Solutions that did not converge with this number of iterations are given a value of 10. If solutions began to diverge or exceeded the critical velocity, a value of the last iteration plus 10 is assigned. A critical velocity requirement is necessary to prevent numerical simulation of a hyperbolic trajectory. These trajectories will never fall back to the surface of rotating body, and thus will always fail to converge. Here critical velocity² is defined as 16 where R_{Earth} is the radius of the spherical body.

$$V_{crit} = \sqrt{\frac{2\mu}{R_{\text{Earth}}}} \quad (16)$$

Using this requirement, resultant corrected velocities exceeding the critical velocity will result in the

iteration loop termination and a value of 10 added.

Hybrid techniques placing the analytical and numerical solutions inside the iterative loops are also examined. These hybrids employ the STM at the beginning of the internal processing loop of the velocity correction and internal comparison of error.

The solutions are further examined using the time required to attempt a solution for each grid point. This examination is subjective, however, to the available computing resources and is not directly repeatable. Solutions are examined as far as determining the inclination of the suborbital trajectory's plane and the angular distance between surface locations in order to determine discontinuities. These discontinuities would result when solutions would fail to converge and errors are large. When drag is introduced, the computational requirement is observed to increase by nearly three orders of magnitude, and rate of failure to converge rapidly increases.

Rotation Effects

The addition of rotation is the first level of complexity added to the basic ballistic missile problem. Target sites will move as the Earth rotates during the period of flight. These target sites therefore must be led in order to hit them after the missile's time of flight. An exact analytic solution exists for this constant flight time problem to account directly for the amount of rotation the Earth during this period.⁴ Thus, pure rotation is seen as a good baseline for an initial comparison, and this method is employed to determine what the final coordinates of the target location are after the flight time of the vehicle. This method is used throughout the simulation as flight time is refined to reflect the flight time necessary to hit inside the target ring of accuracy. With these tools, we initiate our simulation with $\beta = \infty$ to account for the rotational effects. Shown in Figure 3 we see that rotational error exceeds over 1000 km in direct normalized vector form when nearing 180° of angular distance shown in Figure 4.

We note that darker regions have increased error and the darkest regions exceed error of 1000 km. Error also is symmetrical as we should expect. Also, error at the poles is virtually zero since targets located precisely at the poles do not rotate. Values from the simulation indicate error on the order of 1×10^{-6} are accounted. Internal storage of values throughout the numerical integration process appears to be the cause of this discrepancy.

We also examine the case for launch location of 45° N 0° E. We notice here that the angular range will increase diagonally and thus the two-body solution's error due to rotation will increase in these regions. Figure 5 shows the southward trend of error as the launch location is shifted northward. We also note the change in the contour to bulge towards the prime meridian.

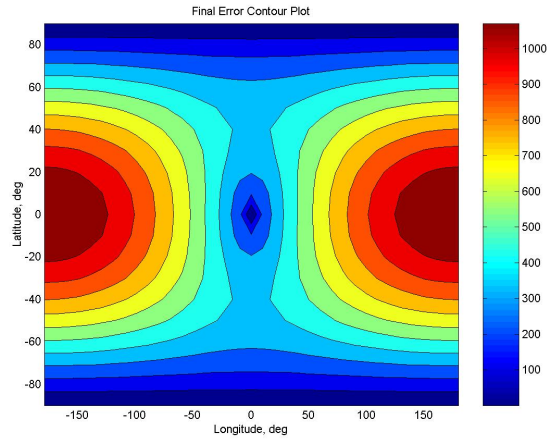


Fig. 3 Plot of error accumulated from pure rotation when launching from a 0° N 0° E using uncorrected initial velocity provided by the two-body solution.

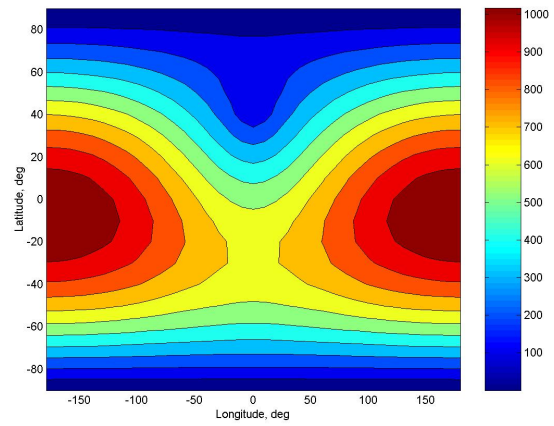


Fig. 5 Error contour plot for launch location 45° N 0° E for solutions uncorrected initial velocity provided by the two-body solution. This plot contains data for the 703 point target array $\beta = \infty$.

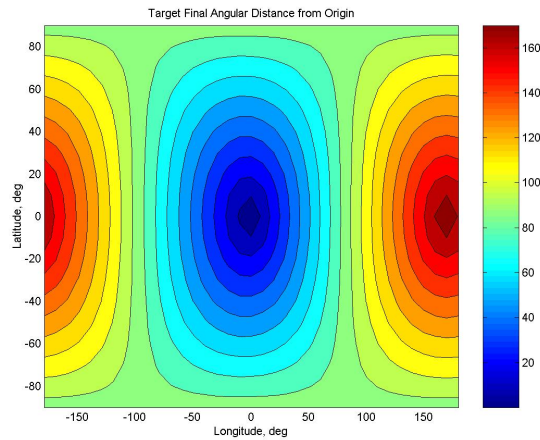


Fig. 4 Plot of angular distance between the launch location 0° N 0° E and the final target locations in the 703 point array. Original positions shift in longitude easterly with rotation during the time of flight. Two-body conditions are provided for the $\beta = \infty$ case.

This trend continues with increasing latitude of the launch site.

Analytical Method

The analytical STM method was utilized in order to create the velocity correction necessary to hit the moving target. Figure 6 depicts the number of iterations required across the 703 point grid array.

The iteration contour map includes the colorbar legend denoting increasing iterations with increasing darkness. As shown, the regions between -150° W and 150° E have a difficult time converging. To understand why there is such a difficulty the angular distance between the origin and the target site following rotation is analyzed.

We review the angular range of the region where solutions fail to converge (10+ iterations) and determine

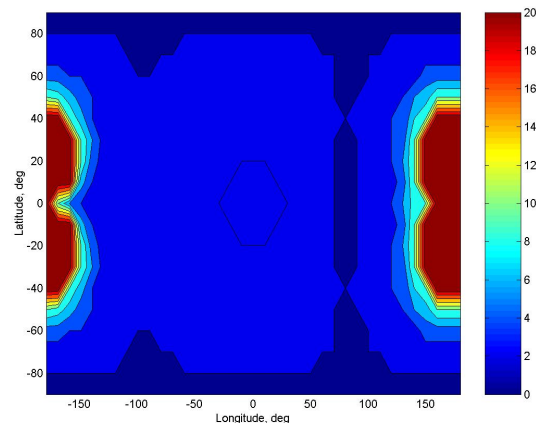


Fig. 6 Iteration contour plot for launch location 0° N 0° E for solutions using the Analytic STM method for the 703 point target array $\beta = \infty$.

that these targets are near 180° . For the minimum energy solution for 180° , the trajectory runs precisely along the surface of the planetary body, or otherwise the apogee altitude is 0 km above the surface. Thus solutions would be difficult to formulate using the minimum energy assumption for this angular range. Figure 7 depicts a transitional boundary where the path switches from posigrade (eastward) to retrograde (westward) trajectories. This boundary seems to well define the region where iterations increase and has the most direct correlation to the increase in required iterations.

As indicated in Figure 7, the band of trajectories using 0° inclination is depicted as a narrow gap approaching 160° E. This correlates to the narrow region of convergence that penetrates the iteration contour plot in the same area. Similarly a region exists for 180° of inclination on the western portion of the grid. The solution seems to break down earlier on the east-

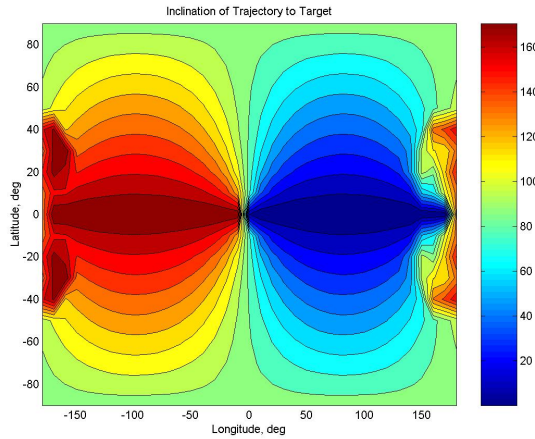


Fig. 7 Inclination contour plot for launch location 0° N 0° E for solutions using the Analytic STM method for the 703 point target array $\beta = \infty$.

ern side of the plot than the western side. This may be attributed to the fact that the eastern portion of the map has a higher angular displacement of the solution. Launching eastward is a more difficult task to catch up to a surface point near 180° than if launching westward. Here the iteration method is switching between launching eastward and westward and having difficulty resolving a solution since large velocity changes are required to completely change direction and thus a large number of iterations.

External Numerical Method

The external numerical STM method is then examined for the rotation only case to determine its effectiveness. We determine that the numerical method produces very similar plots to the analytic method, however, they differ in important ways. Shown in Figure 8, we see that some escape cases are not present. While, the general trend to increase does seem similar, several regions converge using the external numerical STM where the external analytic solution could not. On average the pure numerical STM requires nearly twice as much computing time to complete the simulation than does the pure external analytic STM method at this ballistic coefficient.

Internal Methods

An alternative approach was conceived to determine whether a reformulation of the STM would be appropriate and even assist increasing the speed in which the process would resolve a solution. Here the STM will now be calculated inside the iteration loop shown in Figure 2. The process will now utilize a STM to initially correct the velocity and then lead to reanalysis of error.

The internal methods created errors where the angular phase was nearly 180° . At these phase angles the constraint that the trajectory must not fly through the central body is encountered often with velocity correc-

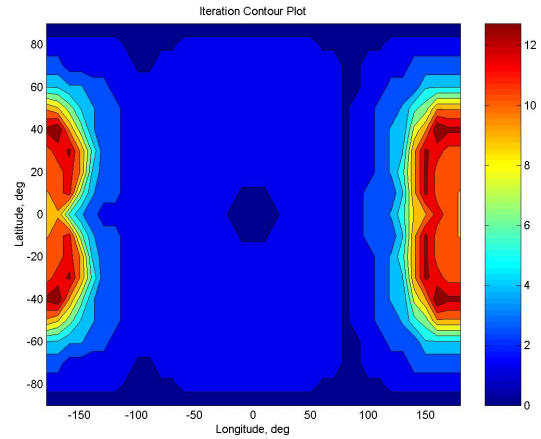


Fig. 8 Iteration contour plot for launch location 0° N 0° E for solutions using the External Numeric STM method for the 703 point target array $\beta = \infty$.

tions. Thus, for these cases, a different initial solution is more appropriate that has a very large apogee altitude. In the next level of fidelity, the atmosphere, the target array is condensed to avoid problems by flying too shallow in the atmosphere.

Atmospheric Effects

The addition of atmospheric effects began by defining the ballistic coefficient. The first case examined is $2 \times 10^{12} \frac{\text{kg}}{\text{km}^2}$. This value is very large for any vehicle, but is a good introduction to the effects of drag, and provides a check if drag in the model that is working correctly. Shown in Figure 9 is the uncorrected velocity as derived from the two-body non-rotating solution.

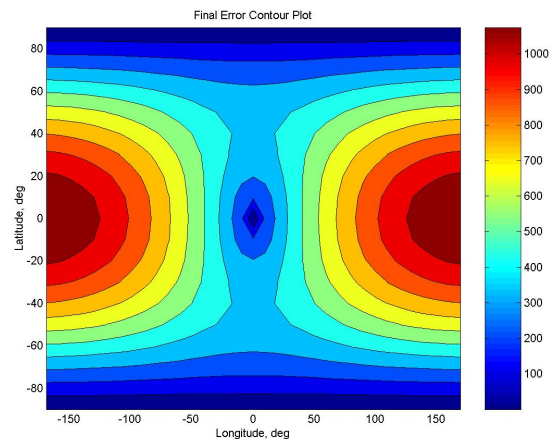


Fig. 9 Error contour plot for launch location 0° N 0° E for solutions uncorrected initial velocity provided by the two-body solution. This plot contains data for the 703 point target array $\beta = 2 \times 10^{12}$.

We notice that is is virtually identical to the $\beta = \infty$ case and when examining the iteration plots 6 and 8 we see that the target array is within 2 iterations for these methods.

Next the $\beta = 2 \times 10^9$ case is explored. Figure 10

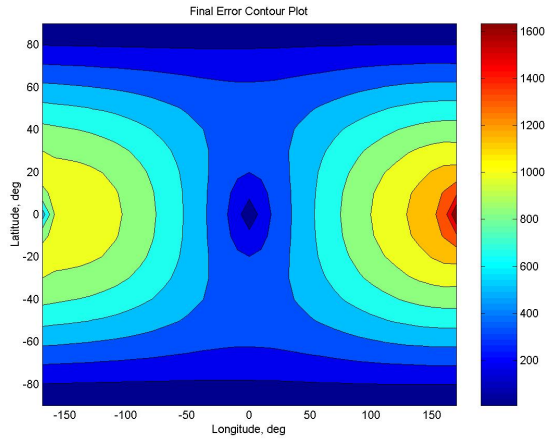


Fig. 10 Error contour plot for launch location 0° N 0° E for solutions uncorrected initial velocity provided by the two-body solution. This plot contains data for the 703 point target array $\beta = 2 \times 10^9$.

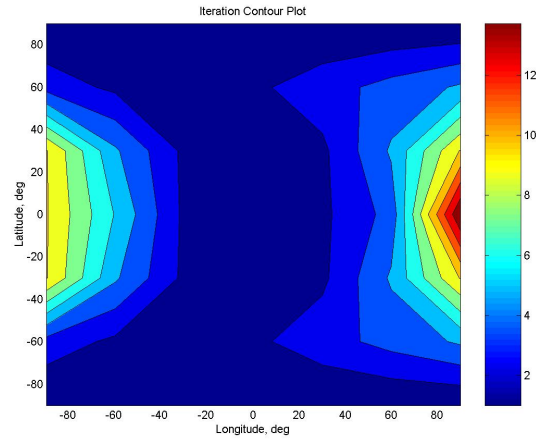


Fig. 12 External Numerical STM iteration contour plot for launch location 0° N 0° E. This plot contains data for the 49 point target array $\beta = 2 \times 10^9$.

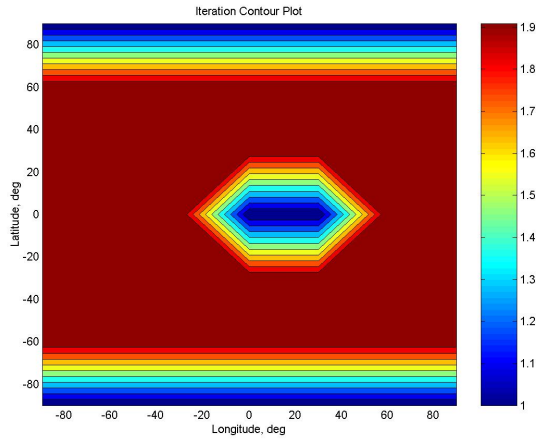


Fig. 11 External Analytic STM iteration contour plot for launch location 0° N 0° E. This plot contains data for the 49 point target array $\beta = 2 \times 10^9$.

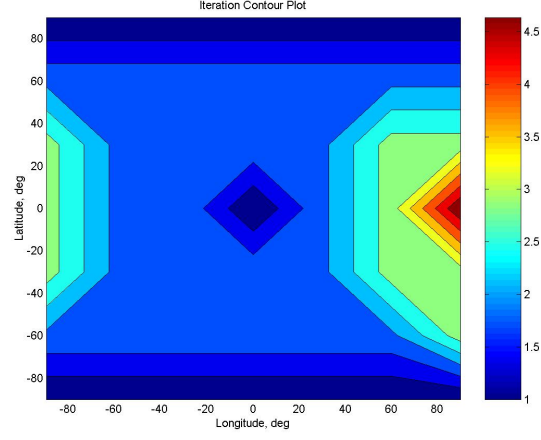


Fig. 13 Internal Numerical STM iteration contour plot for launch location 0° N 0° E. This plot contains data for the 49 point target array $\beta = 2 \times 10^9$.

shows the uncorrected error on the non-rotating two body solution. Here we notice that error increases significantly and note the change in scale on the colorbar from the previous example.

Analytical Methods

The analytical methods both external and internal are again used to determine their effectiveness. Not surprisingly they again result in the same number of iterations with the internal method having less error at the conclusion. Figure 11 shows the resultant iteration contour plot. Again the analytic method has little problem in resolving a solution within this target regime.

Numerical Methods

Next, the numerical cases are explored. First the external numerical method is employed to determine its effectiveness. The resultant contour plot is show in

Figure 12.

Next, the internal method is used. Figure 13 shows that the number of iterations are significantly lower than the external method, and produce better results where cases converge in the internal method where in the external method they do not.

Lastly, the $\beta = 200 \times 10^6 \frac{\text{kg}}{\text{km}^2}$ case is examined. Since we already know significant errors are being introduced at longer angular ranges for the previous case, we can expect even more failures (iterations exceeding 10) to occur in the numerical cases as noted in Figure 12. The functions internal to the program appear to break down at this level for reasons not fully understood. Research into better techniques using numerical propagators with error detection will be conducted in the future.

The analytic solutions however, provided excellent solutions to this level of the drag problem. It appears that the effects of rotation are in many ways similar

to the effects of drag as used in this model, and can be resolved at this value of β .

Figure 14 shows the uncorrected error resultant from the two-body initial guess. Error approaches 2000 km for the cases near 150° E and W longitude while error for the region of study is near 1200 km.

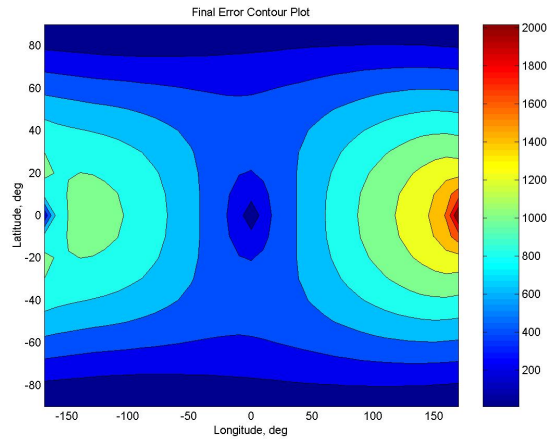


Fig. 14 Error contour plot for launch location 0° N 0° E for solutions uncorrected initial velocity provided by the two-body solution. This plot contains data for the 703 point target array $\beta = 200 \times 10^6$.

Since the analytic solutions both converged within 2 iterations in a similar fashion, the final error is compared between the internal and external methods. First we show the external method in Figure 15, we see that it is near 1.2 km on the east and west boundaries of the region of study.

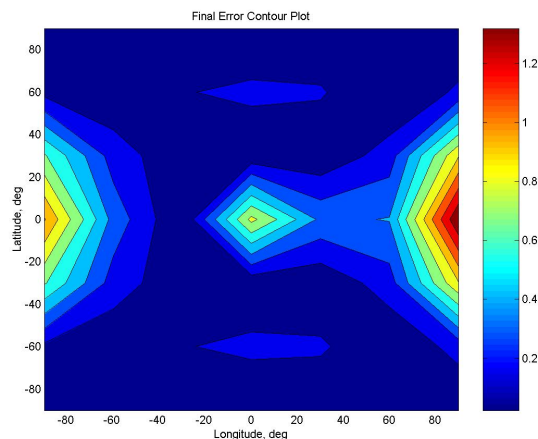


Fig. 15 External Analytic STM error contour plot for launch location 0° N 0° E. This plot contains data for the 49 point target array $\beta = 200 \times 10^6$.

Next we examine the internal method shown in Figure 16. Here we see that error has dropped below 0.3 km thus demonstrating the usefulness of using the STM internally to drive error to 0 more effectively.

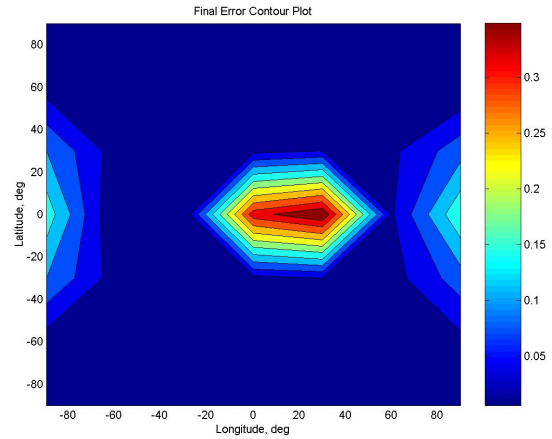


Fig. 16 Error contour plot for launch location 0° N 0° E for solutions Internal Analytic STM. This plot contains data for the 49 point target array $\beta = 200 \times 10^6$.

Conclusions and Future Work

Both the numerical and analytical methods have their merits. The numerical method is robust in some cases when the analytical solution breaks down. Internal methods are more computationally expensive than are external methods that are only implemented once. The analytic method is calculated with the same speed at every iteration for all values of β while the numerical method is slowed significantly as β decreases. The analytic method has proven especially useful for accounting for drag in this setup. This seems to be due to the fact that the additional flight time required to proceed around the spherical body is not nearly as significant as are effects of the rotation. Since the projectile's studied still had high values of ballistic coefficient, they were not slowed by a large fraction of their velocity at the interface with the significant atmosphere.

The numerical solutions will require further study. Numerical methods break down earlier than analytic solutions in the current formation of the implemented code. Further research will be conducted in the future to make these methods more robust and fault proof. Different numerical integration methods will also be researched in further detail as well as the application of the event detection method used to create the spherical surface constraint. Effects of J_2 will also be examined, though anticipated to be minimal for these relatively short flight times. Drag modulated and lift modulated re-entry vehicles will also be investigated and modelled in future work to create a flexible dynamics program.

References

- ¹Miele, A., *Theory of Flight Paths*, Vol. 1., Addison-Wesley Publishing Company, Palo Alto.
- ²Schaub, H. and Junkins, J., *Analytical Mechanics of Space Systems*, AIAA Education Series, Reston, VA, 2003.
- ³Battin, R. H., *An Introduction to the Mathematics and*

Methods of Astrodynamics, AIAA Education Series, New York, 1987.

⁴Bate, R. R., Mueller, D. D., and White, J. E., *Fundamentals of Astrodynamics*, Dover Publications Inc., New York, 1971.

⁵McFarland, J. S., "Dynamic Sensitivity Considerations of Non-Lifting Ballistic Re-Entry Vehicles," AIAA Region I - NE and MA, College Park, Maryland, April 11-13 2003.

⁶Loh, W. H. T., "Dynamics and Thermodynamics of Re-Entry," *Journal of the Aerospace Sciences*, Vol. 27, 1960, pp. 748-762.

⁷Regan, F. J. and Anandakrishnan, S. M., *Dynamics of Atmospheric Re-Entry*, American Institute of Aeronautics and Astronautics (AIAA), Washington, DC, 1993.

⁸Wertz, J. and Larson, W., editors, *Space Mission Analysis and Design*, Space Technologies Series, Microcosm Press and Kluwer Academic Publishers.

⁹Larson, W. and Pranke, L. K., editors, *Human Space Mission Analysis and Design*, Space Technologies Series.